Efficient electron dynamics with the planewave-based real-time time-dependent density functional theory: Absorption spectra, vibronic electronic spectra, and coupled electron-nucleus dynamics

Seung Kyu Min, Yeonchoo Cho, and Kwang S. Kim

Citation: The Journal of Chemical Physics **135**, 244112 (2011); doi: 10.1063/1.3671952

View online: http://dx.doi.org/10.1063/1.3671952

View Table of Contents: http://scitation.aip.org/content/aip/journal/jcp/135/24?ver=pdfcov

Published by the AIP Publishing

Efficient electron dynamics with the planewave-based real-time time-dependent density functional theory: Absorption spectra, vibronic electronic spectra, and coupled electron-nucleus dynamics

Seung Kyu Min, Yeonchoo Cho, and Kwang S. Kim[a)]
Center for Superfunctional Materials, Department of Chemistry, Pohang University of Science and Technology, San 31, Hyojadong, Namgu, Pohang 790-784, Korea

(Received 10 August 2011; accepted 5 December 2011; published online 30 December 2011)

The electron dynamics with complex third-order Suzuki-Trotter propagator (ST_3) has been implemented into a planewave (PW) based density functional theory program, and several applications including linear absorption spectra and coupled electron-nucleus dynamics have been calculated. Since the ST_3 reduces the number of Fourier transforms to less than half compared to the fourth-order Suzuki-Trotter propagator (ST_4), more than twice faster calculations are possible by exploiting the ST_3. We analyzed numerical errors of both the ST_3 and the ST_4 in the presence/absence of an external field for several molecules such as Al_2, N_2, and C_2H_4. We obtained that the ST_3 gives the same order of numerical errors (10^{-5} Ry after 100 fs) as the ST_4. Also, the time evolution of dipole moments, hence the absorption spectrum, is equivalent for both ST_3 and ST_4. As applications, the linear absorption spectrum for an ethylene molecule was studied. From the density difference analysis, we showed that the absorption peaks at 6.10 eV and 7.65 eV correspond to the $\pi \rightarrow 4a_g$ and $\pi \rightarrow \pi^*$ excitation bands, respectively. We also investigated the molecular vibrational effect to the absorption spectra of an ethylene molecule and the dynamics of a hydrogen molecule after the $\sigma \rightarrow \sigma^*$ transition by formulating coupled electron-nucleus dynamics within the Ehrenfest regime. The trajectory of nuclei follows the excited state potential energy curve exactly. © *2011 American Institute of Physics*. [doi:10.1063/1.3671952]

I. INTRODUCTION

Understanding the interaction between light and materials has been of great importance in chemistry, physics, and biology. It naturally involves excited states where traditional ground state (GS) theories fail and thus the method for excitations is required.[1,2] The linear response time-dependent density functional theory (TDDFT) pioneered by Gross and Kohn[3] becomes the most popular method to calculate the excitation energies.[4–11] However, it is limited to investigate the response of electron density beyond the linear response, according to the applied perturbation, and can be described regardless of the strength of the perturbation. To this end, the real-time time-dependent density functional theory (RT-TDDFT),[12–26] a real-time approach in TDDFT regime,[27] is proposed to investigate the "real" electron dynamics according to the applied external field.

RT-TDDFT enables electron dynamics simulations which has been intractable due to theoretical and computational limitations. As a TDDFT-based electron dynamics method, it has several advantages. First, as mentioned above, this is a non-perturbative approach and can deal with nonlinear phenomena. Second, the development of "attosecond spectroscopy"[28–30] makes possible to measure the real-time motion of electrons, where RT-TDDFT may help understand those ultrafast phenomena. Finally, the computational methods describing light-induced chemical reactions by Ben-Nun, Martinez, and Tully[31–33] deal with the nucleus motion on the exact excited state potential energy surface. The RT-TDDFT coupled to the nucleus motion can describe the excited state dynamics efficiently.

In accordance with these advantages, several RT-TDDFT implementations have been demonstrated in recent years. They are different in the basis set and the propagation operator. Sugino and Miyamoto have developed PW-based electron dynamics program using the self-consistent ST_4 operator,[16] and have studied the behavior of electron propagation in the condensed matter system.[18,19] Yabana *et al.* and Castro *et al.* have solved the RT-TDDFT in numerical grids, and obtained successful absorption spectra of several molecules.[12–15] For the case of atomic orbital basis sets, many researchers have studied excited state properties by using their house-made real-time electron dynamics program.[20–26] Chen *et al.* have implemented classical electrodynamics coupled to quantum electron dynamics, and obtained absorption spectra of a silver nanoparticle absorbed with a molecule.[21] Lopata *et al.* have developed massively parallel RT-TDDFT method and investigated the electron dynamics of an excited zinc porphyrin.[22] Also, there are many efforts to couple the motion of nuclei to electron dynamics.[26,27]

Even though there are many efforts to implement the RT-TDDFT on various density functional theory (DFT)-based programs, the faster and accurate numerical time evolution is always important for the practical RT-TDDFT. Here, we adopt planewave basis and the Suzuki-Trotter (ST) time evolution operators. Planewave basis allows us to deal with elec-

a)Electronic mail: kim@postech.ac.kr.

trons escaping from nuclear potential, where atom-centered basis faces obvious limitation. The Suzuki-Trotter propagator is the most suitable for planewave basis. Moreover, it is numerically stable, allows systematic improvements, and satisfies unitarity and time-reversal symmetry.[34] Numerical stability is crucial since the simulation over hundreds of thousands time steps should be achieved to describe proper excited state phenomena which occur for a few to hundreds of femtoseconds. Sugino and Miyamoto also adopted planewave with the propagator. However, we implemented improved ST operator with complex time propagation and thereby achieved faster and more reliable simulations.

In this paper, we present an efficient algorithm for the RT-TDDFT in the PW-based code, quantum-ESPRESSO,[35] with the complex time domain ST propagator.[36] We investigate the accuracy and stability of the present method with/without an external field as compared to the real time propagation with the higher order ST propagator.[16,37] As test examples, first, the linear absorption spectrum of an ethylene molecule is obtained as a result of the electron dynamics. Second, implementing the coupled electron-nucleus dynamics within the Ehrenfest regime,[38] the dissociation of the excited hydrogen molecule is studied.

II. METHODS

A. Theoretical basis

First, we briefly introduce the RT-TDDFT. The RT-TDDFT begins with the time-dependent Kohn-Sham (TDKS) equation and the time-dependent electron density (ρ) obtained from the Kohn-Sham (KS) orbitals (ϕ_i's) in Eq. (1).

$$i\frac{\partial}{\partial t}\phi_i(\mathbf{r},t) = h_{\mathrm{KS}}(\mathbf{r},t)\phi_i(\mathbf{r},t),$$
$$\rho(\mathbf{r},t) = \sum_i^{occ} |\phi_i(\mathbf{r},t)|^2. \quad (1)$$

Here, TDKS Hamiltonian (h_{KS}) is represented by

$$h_{\mathrm{KS}}(\mathbf{r},t) = -\frac{1}{2}\nabla^2 + v_{\mathrm{KS}}(\mathbf{r},t)$$

where

$$v_{\mathrm{KS}}(\mathbf{r},t) = v_{\mathrm{H}}[\rho(\mathbf{r},t)] + v_{\mathrm{xc}}[\rho(\mathbf{r},t)] + v_{\mathrm{ext}}(\mathbf{r},t). \quad (2)$$

We should note that a KS orbital need not be an eigenfunction of h_{KS}(**r**,t) any longer, rather it is a basis function to span the electron density. The KS potential (v_{KS}) consists of the Hartree potential (v_{H}), the exchange-correlation potential (v_{xc}), and the external potential (v_{ext}). As in the static DFT, the exact exchange-correlation functional v_{xc} should be approximated. We use the adiabatic local density functional approximation (ALDA).[39] The external potential v_{ext} contains potentials from nuclei (v_{N}) and time-dependent external fields (v_{field}). The total electronic energy is calculated by using

$$E_{\mathrm{total}}(t) = \sum_i^{occ} \langle\phi_i(t)|\, h_{\mathrm{KS}}\, |\phi_i(t)\rangle - \int d\mathbf{r}\ [v_{\mathrm{Hartree}} + v_{\mathrm{xc}}] \times \rho(\mathbf{r},t) + E_{\mathrm{xc}} + E_{\mathrm{H}} + E_{\mathrm{ext}}, \quad (3)$$

where E_{xc}, E_{H}, and E_{ext} are the exchange-correlation, Hartree, and external energy, respectively, from ρ(**r**,*t*). Compared to the normal GS electronic energy, the only difference is the use of expectation values instead of KS energies.

Practically, we solve the integral equation with the time evolution operator $U(t+\Delta t,t)$ instead of Eq. (1):

$$\phi_i(t+\Delta t) = U(t+\Delta t, t)\phi_i(t),$$

where

$$U(t+\Delta t, t) \equiv \hat{T}\exp\left[-i\int_t^{t+\Delta t} dt\ h_{\mathrm{KS}}(t)\right]. \quad (4)$$

Here, $\hat{T}$ is a time ordering operator. Then, all we have to do is to build the numerical time evolution operator to generate KS orbitals at the next time step.[40] Numerical methods to solve the above TDKS equation have been studied based on various quantum computational codes.[12–26] However, the details are quite different depending on the basis sets. In this paper, we focus on the PW-based code.

B. Calculations

Since we should use the pseudopotential (PP) in the PW-based code for the sake of the efficiency, v_{KS} can be divided into local and non-local terms: the local potential (v_L) contains v_{H}, v_{xc}, v_{field}, and the local part of PPs, while the non-local potential (v_{NL}) attributes to the remaining part of PPs:

$$v_{\mathrm{KS}}(\mathbf{r},t) = v_L + v_{NL}. \quad (5)$$

Thus, the KS Hamiltonian consists of three components: kinetic (T), local potential (V_L), and nonlocal potential (V_{NL}) parts. Since the kinetic part and the local potential can be represented easily in the reciprocal space and the real space, respectively, the ST method which is based on the split operator technique is a good candidate for the replacement of $U(t+\Delta t,t)$ in Eq. (4).[16,37] Generally, the parameters for the ST method are chosen as real, thus, the KS orbitals are evolved in the real time axis. In the case of the PW basis set, the most time-consuming and error-generating step is the fast Fourier transform (FFT). Here, we implemented the accurate but fast time evolution for the PW-based code with the complex ST_3 which reduces the number of the FFT operations drastically. Prosen and Pižorn reported that the third-order ST operation with the renormalization in the complex time domain gives the same accurate results as the ST_4 operation in the real time axis due to the Hermitian property of Hamiltonian.[36] The ST_4 with the KS Hamiltonian is represented as

$$\mathrm{ST}_4(z) \equiv \mathrm{ST}_2(r_1 z)\mathrm{ST}_2(r_1 z)\mathrm{ST}_2(r_2 z)\mathrm{ST}_2(r_1 z)\mathrm{ST}_2(r_1 z)$$

where

$$r_1 = 1/(4-4^{1/3})$$

and

$$r_2 = 1 - 4r_1, \quad (6)$$

while the ST_3 is

$$\mathrm{ST}_3(z) \equiv \mathrm{ST}_2(c_1 z)\mathrm{ST}_2(c_2 z)$$

where

$$c_1 = c_2^* = 1/4 + \sqrt{3}/12i. \quad (7)$$

Here, the second order ST operator, ST_2, is

$$ST_2(z) \equiv e^{zT/2} e^{zV_{NL}/2} e^{zV_L} e^{zV_{NL}/2} e^{zT/2}$$

where

$$z = i\Delta t. \tag{8}$$

Note that two time steps and the renormalization are required to achieve unitarity. Indeed, ST_3 for a single time step does not satisfy the unitarity relation due to the imaginary time. However, unitarity can be achieved within two time steps if we choose c_1 (thus c_2) for the subsequent time evolution (from $t + \Delta t$ to $t + 2\Delta t$) as a complex conjugate of the former c_1 (thus c_2), and renormalize the wavefunction after $t + 2\Delta t$. The exponent of V_L is located at the center of ST_2 to minimize the number of FFTs. The operation of each component (e^{zA}) on a certain function in Hilbert space ($f(\mathbf{r})$ or $\mathbf{f}$) should be calculated to obtain $\phi_i(t + \Delta t)$ in Eq. (4). For the case of $A = V_L$, $e^{zV_L}\mathbf{f}$ should be calculated in real space via FFT. The operation is a simple multiplication of $e^{zV_L(\mathbf{r})}$ and $f(\mathbf{r})$ in real space, and $e^{zV_L}\mathbf{f}$ can be obtained from its inverse FFT. The nonlocal potential Hamiltonian V_{NL} within separable form of norm-conserving PPs can be divided into the sum of PPs from each nucleus. Then, we approximate the total exponential of V_{NL} as the product of the exponentials of V_{NL}^a where a is the nucleus index:

$$e^{zV_{NL}} = e^{z\sum_a V_{NL}^a} \simeq \prod_a e^{zV_{NL}^a}. \tag{9}$$

In norm-conserving PPs, the operation of non-local potentials on the wavefunction can be represented as

$$V_{NL}^a |\psi_i\rangle = \sum_{n,m\in a} |\beta_n\rangle B_{nm}^a \langle\beta_m|\psi_i\rangle . \tag{10}$$

The meaning of $|\beta_n\rangle$ and B_{nm}^a can be found in Ref. 41 which is another representation of normal norm-conserving PP equation,

$$V_{NL}^a = \sum_{i\in a} \frac{|\chi_i\rangle \langle\chi_i|}{\langle\chi_i \mid \phi_i\rangle}, \tag{11}$$

where $|\chi_i\rangle$ and $|\phi_i\rangle$ are a local wavefunction and a pseudowavefunction, respectively.

Here, the matrix element B_{nm}^a is determined by the type of a nucleus, while the projection vector $|\beta_n\rangle$ depends on the position of nuclei. Since the matrix $\mathbf{B}^a$ is a diagonal matrix, the exponent can be easily calculated.

For the sake of accuracy, the change of local potential V_L in Eqs. (6) and (7) due to the rapid oscillation of electron density should be considered. Applying the railway interpolation scheme,[16] we can interpolate potential energies at the intermediate times, t_m's, by using old and new potentials and their derivatives (Eq. (12)):

$$\begin{aligned} V_L(t_m) = &\left(\frac{t_m - t - \Delta t}{\Delta t}\right)^2 \left[3V_L(t) + \Delta t \dot{V}_L(t) \right. \\ &\left. + \frac{t_m - t - \Delta t}{\Delta t}\left[2V_L(t) + \Delta t \dot{V}_L(t)\right]\right] \\ &+ \left(\frac{t_m - t}{\Delta t}\right)^2 \left[3V_L(t + \Delta t) - \Delta t \dot{V}_L(t + \Delta t) \right. \\ &\left. - \frac{t_m - t}{\Delta t}\left[2V_L(t + \Delta t) - \Delta t \dot{V}_L(t + \Delta t)\right]\right]. \end{aligned} \tag{12}$$

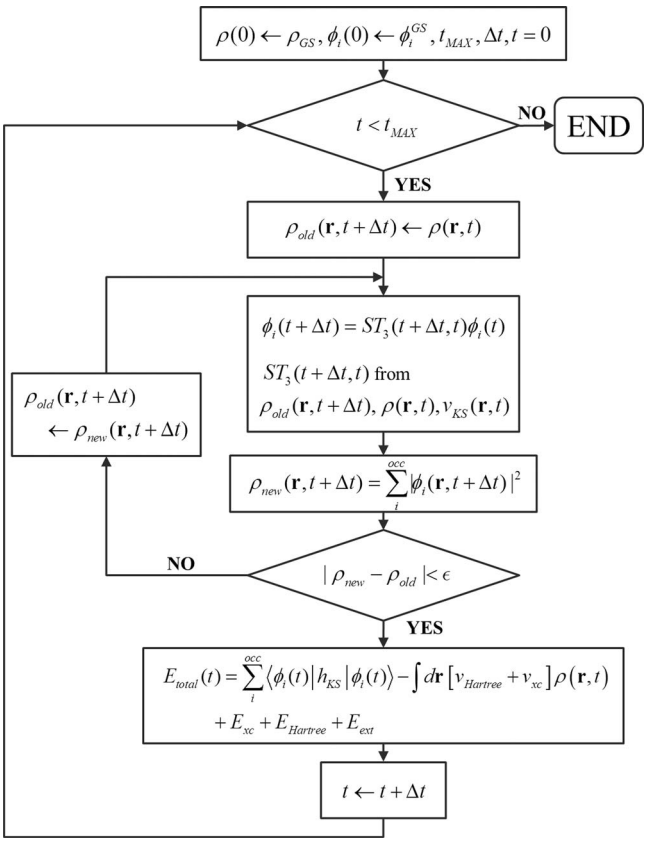

FIG. 1. A flow diagram for the RT-TDDFT method.

From the adiabatic and local approximation such as ALDA, the time derivative of potential can be derived from the simple multiplication of the time derivative of electron density ($\dot{\rho}$) and the functional derivative of potential over electron density:

$$\dot{V}_L(\mathbf{r}, t) = \int d\mathbf{r}' dt' \frac{\delta V_L(\mathbf{r}, t)}{\delta\rho(\mathbf{r}', t')} \dot{\rho}(\mathbf{r}', t') = \frac{\delta V_L(\mathbf{r}, t)}{\delta\rho(\mathbf{r}, t)} \dot{\rho}(\mathbf{r}, t). \tag{13}$$

The second equality in Eq. (13) only holds for the local exchange-correlation functional approximation for both time t and position $\mathbf{r}$. $V_L(t + \Delta t)$ is equal to $V_L(t)$ initially, and the newer $V_L(t + \Delta t)$ can be obtained from newly calculated $\phi_i(t + \Delta t)$ in Eqs. (6) and (7). Until the self-consistency is satisfied, this cycle should be repeated. Fortunately, the self-consistency is usually satisfied within only a few cycles due to the small size of Δt. The overall flow chart for the RT-TDDFT is depicted in Fig. 1. Here, the only difference from the GS-DFT is obtaining electron density not from the diagonalization but from the time evolution.

III. RESULTS

A. Accuracy and stability

Considering the atomic unit of time (~24 attoseconds), Δt should be an order of attoseconds. Since the photochemical reactions occur within hundreds of femtoseconds, the real-time simulation over hundreds of thousands electronic time steps should be required. Noting that ST_4 contains at least five exponents of V_L (Eq. (12)), the ST_3 in the present

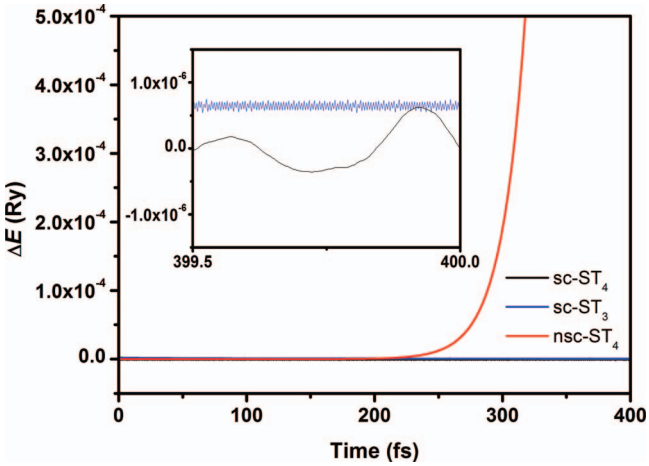

FIG. 2. Time evolution of the numerical error $\Delta E = E_{\text{total}}(t) - E_{\text{total}}(0)$ for the Al_2 case. Both the self-consistent calculations for ST_4 (black) and ST_3 (blue) show accurate and steady results, while the non-self-consistent result (red) shows the catastrophic divergence after the long time simulation. The RMS of the numerical errors for sc-ST_3 is 9.5×10^{-7} Ry while the RMS for sc-ST_4 is 7.4×10^{-7} Ry after 500 fs. The inset shows the ΔE's for sc-ST_3 and sc-ST_4 from 399.5 fs to 400 fs.

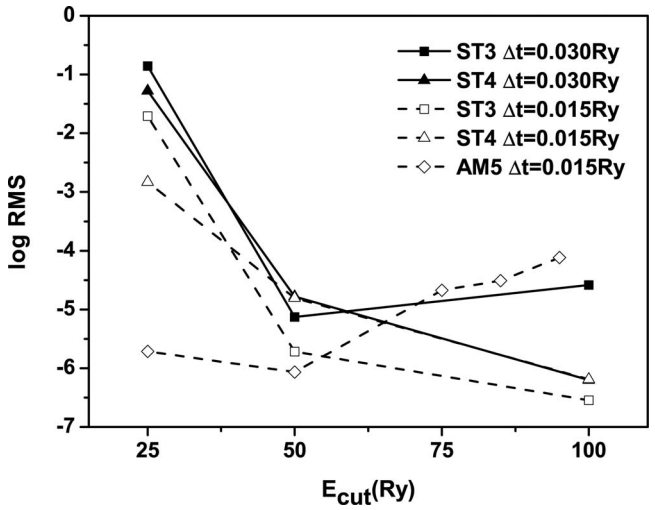

FIG. 3. The time step size (Δt) and kinetic energy cutoff (E_{cut}) dependency of numerical errors for ST_3, ST_4, and AM_5 integrators.

method which contains only two exponents of V_L may give twice faster results as well. Here, we investigate the accuracy of ST_3 compared to ST_4. We define the numerical errors of the time evolution method as $\Delta E = E_{\text{total}}(t) - E_{\text{total}}(0)$ in the absence of the external field. Figure 2 shows the numerical errors of the self-consistent ST_3 and the (non) self-consistent ST_4. Here, we study the ground state electron dynamics for the aluminium dimer (Al_2) with the cutoff of 50 Ry using Troullier-Martin PPs.[42] With the time step of 2.4 attoseconds, the simulation over 200 000 time steps (~500 fs) was performed. With the self-consistent method, both ST_3 and ST_4 give stable results, while the non-self-consistent result suffers from a catastrophic divergence after the long time simulation. The root-mean-square (RMS) of ΔE for the self-consistent ST_3 (sc-ST_3) is 9.5×10^{-7} Ry, while that for the self-consistent ST_4 (sc-ST_4) is 7.4×10^{-7} Ry. The RMS for C_2H_4 shows 2.4×10^{-6} Ry for sc-ST_3 and 1.9×10^{-6} Ry for sc-ST_4 after 100 fs. The RMS values for both ST_3 and ST_4 would be overall equivalent. In certain cases like N_2, the RMS for sc-ST_3 is 1.3×10^{-6} Ry which is much smaller than 1.2×10^{-5} for sc-ST_4 after 100 fs.

Figure 3 shows the dependency of numerical errors in ground states for various time evolution methods on Δt and planewave kinetic energy cutoff, E_{cut}. Here, a fifth-order Adams-Moulton integrator (AM_5) is a self-consistent version of a fifth-order Adams-Bashford integrator (AB_5) which exploits a linear combination of time derivatives from former five time steps. AB_5 shows a divergent result with charge accumulation or depletion as time passes while AM_5 shows a convergent result. Thus, the results with AB_5 are not depicted in Fig. 3. For both the cases, ST_3 and ST_4, the smaller Δt and the larger E_{cut} give systematically smaller numerical errors. In this case, the condition of $E_{\text{cut}} \geq 50$ Ry gives a satisfactory result for every case with a numerical error less than $\sim 10^{-5}$. For the case of AM_5, however, the larger E_{cut} gives the larger numerical errors. Since AM_5 is not unitary itself, the orthogonal property of time evolved KS wavefunctions is not satisfied. It should be empathized that the AM_5 works only for the smaller time step size compared to ST_3 and ST_4. Also, the convergence of AM_5 is slower than that of ST_4 or ST_3. For the case of a N_2 molecule, $\Delta t = 0.03$ Ry with AM_5 does not satisfy the self-consistent condition. Even though AM_5 which requires only two FFTs is faster than both ST_3 and ST_4 for a single step, AM_5 should be used carefully due to the stability and convergence problems.

We also investigate the energy conservation after a delta-function kick external field, i.e., $\mathbf{E}(t) = \mathbf{E}_0\delta(t)$. In this case, we consider the numerical errors of the time evolution method as $\Delta E = E_{\text{total}}(t) - E_{\text{total}}(0^+)$ since the total energy should be conserved without external fields. The RMS for N_2 shows 2.3×10^{-5} Ry for sc-ST_3 and 4.7×10^{-5} Ry for sc-ST_4 after 100 fs. In case of Al_2, the RMS for sc-ST_3 is 1.9×10^{-7} Ry while the RMS for sc-ST_4 is 4.8×10^{-7} Ry after 100 fs. In Fig. 4, the time evolution of dipole moment of the molecular axis and the spectra for a nitrogen molecule from both sc-ST_3 and sc-ST_4 are depicted. The absorption cross section (σ) can

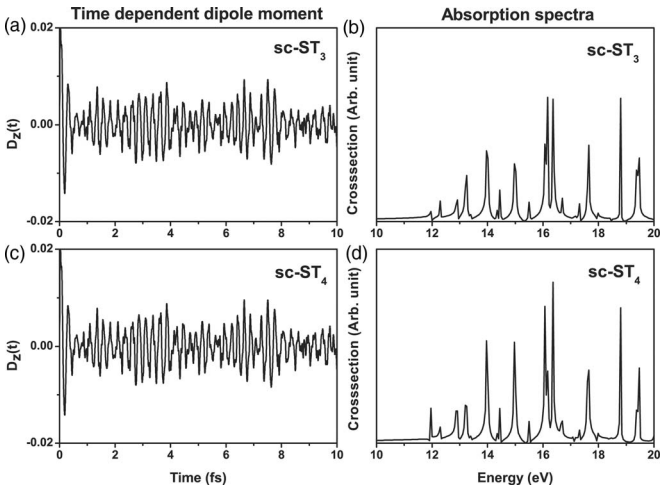

FIG. 4. The time evolution of dipole moments ((a) and (c)) along the molecular axis ($D_z(t)$) and the absorption cross sections ((b) and (d)) for a nitrogen molecule from the sc-ST_3 ((a) and (b)) and the sc-ST_4 ((c) and(d)).

be obtained from the polarizability (α):

$$\sigma(\omega) = \mathrm{Im}\langle\alpha(\omega)\rangle = \frac{1}{3}\mathrm{Im}[Tr\alpha(\omega)], \tag{14}$$

where the relation between polarizability, electric field (**E**), and dipole moment (**d**) is

$$\mathbf{d}(\omega) = \alpha(\omega)\mathbf{E}(\omega). \tag{15}$$

Thus, $\alpha(\omega)$ can be obtained depending on the time-dependency of the applied external field, $\mathbf{E}(t)$. As an example, $\alpha(\omega)$ for the delta-function kick electric field can be written as

$$\alpha_{\mu\nu}(\omega) = -\frac{1}{E_0}\int_0^\infty dt\ e^{i\omega t} d_\mu(t). \tag{16}$$

Both methods show exactly identical behaviors for the time dependent dipole moment and the absorption spectra. Thus, we can conclude that the sc-ST_3 method gives the same result as the sc-ST_4 method with a more than two-times faster algorithm. A particular advantage in ST_3 is that the energy fluctuation for ST_3 tends to be much smaller than ST_4, and so ST_3 shows more steady results. This error which is less than $\sim 10^{-5}$ Ry ($= \sim 1.5$ K) is insignificant. As the time elapses, the error becomes much smaller, and therefore ST_3 is reliable, steady, and accurate. Thus, if one requires very accurate results for a very short time span, ST_4 could be slightly more appropriate. However, for a long time scale, ST_3 is much more favored.

B. Linear absorption spectrum

One of applications in RT-TDDFT is to calculate linear absorption spectra. Here, we calculated linear absorption spectra of an ethylene (C_2H_4) molecule in D_{2h} symmetry. Applying a step function electric field, we obtained the time-dependent electric dipole moment up to 150 fs with a time step size of 1.5 as. Figure 5 shows the calculated absorption cross section from our RT-TDDFT code (top) and from the YAMBO program[43] using the linear response TDDFT (LR-TDDFT) (bottom). Here, σ_x, σ_y, and σ_z are absorption cross sections with an applied electric field along x, y, and z directions, respectively. Both methods show almost identical absorption spectra, while there are slight differences in the high energy region because the linear response spectrum is obtained by including the finite number of unoccupied KS orbitals. According to the selection rule, we can conjecture that σ_z is related to the π-π^* transition. To assign the absorption peak more precisely, we applied the harmonic, or sinusoidal, field along the z-direction with the frequency corresponding to absorption maximum, 7.65 eV. Before doing this, the resonance and off-resonance phenomena depending on the applying frequency were studied (Fig. 6(a)). There is no absorption

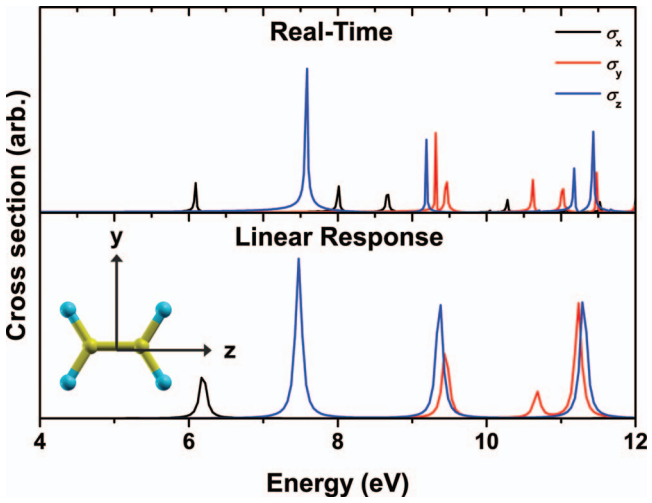

FIG. 5. The calculated linear absorption spectrum with RT-TDDFT (up) and LR-TDDFT (bottom). The σ_x, σ_y, and σ_z are absorption cross sections with an applied electric field along x, y, and z directions, respectively. The ethylene molecule (C_2H_4) with D_{2h} symmetry is also depicted.

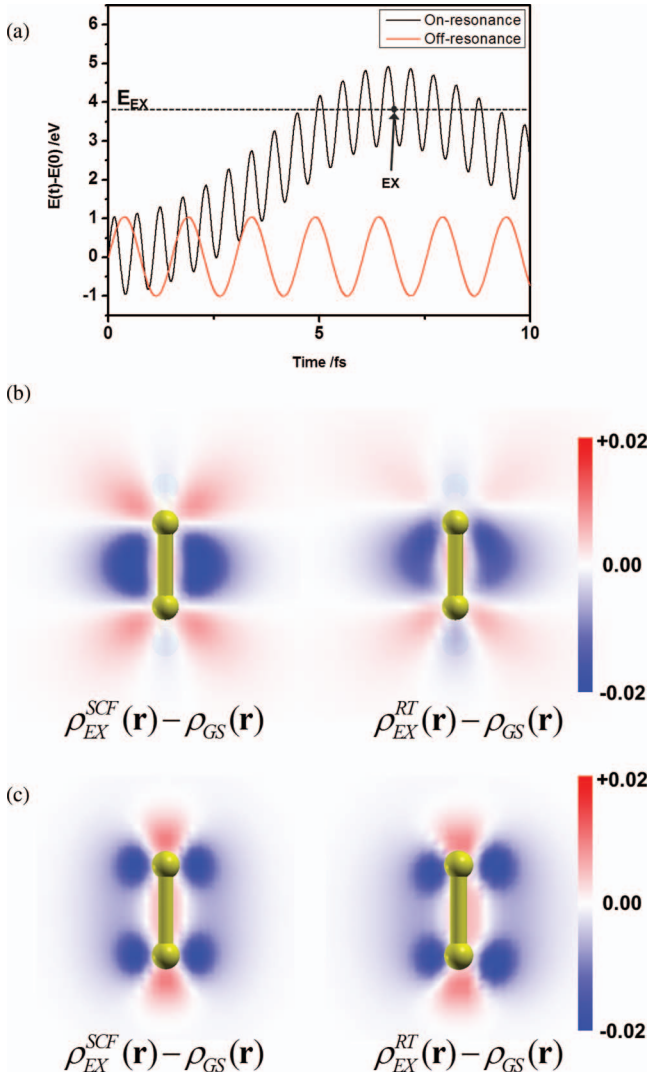

FIG. 6. (a) The on/off-resonance phenomena with the absorption/non-absorption frequency for the ethylene molecule. The on-resonance is obtained by applying the harmonic field with the frequency of 7.65 eV, while the off-resonance is obtained by applying the harmonic field with the frequency of 2.72 eV. ((b) and (c)) The density difference maps between the ground state density ($\rho_{GS}(\mathbf{r})$) and the excited state densities ($\rho_{EX}^{SCF}(\mathbf{r})$ and $\rho_{EX}^{RT}(\mathbf{r})$, which are obtained from the self-consistent calculation with the excited state occupation and from the real-time calculation, respectively) for resonant frequencies as 7.65 eV along z-direction ($\omega_z = 7.65$ eV) (b) and 6.10 eV along x-direction ($\omega_x = 6.10$ eV) (c). Both density difference maps show almost identical behaviors implying that the excitations of $\omega_z = 7.65$ eV and $\omega_x = 6.10$eV correspond to π-π^* and π-$4a_g$ excitations, respectively.

for the off-resonant frequency (2.72 eV), whereas there is energy increase according to the Rabi oscillation formula for the resonant frequency (7.65 eV). Thus, we can say that the ethylene molecule is excited with the resonance frequency. However, we should admit that the discrepancy between E_{EX}-$E(0)$ and the applied frequency is due to the partial excitation from the ground state, giving an energy between the exact excited state and the ground state energy $E(0)$. In this sense, analyzing the density difference map according to the applied harmonic field with an absorbing frequency would be a technique to assign the absorption peaks even though the reference density can be obtained from not the exact excited state wavefunctions but the change of occupation numbers of KS orbitals. The density difference maps between the ground state density $\rho_{GS}(\mathbf{r})$ and the excited state density ($\rho_{EX}^{SCF}(\mathbf{r})$ and $\rho_{EX}^{RT}(\mathbf{r})$, which are obtained from the self-consistent calculation with the excited state occupation and from the real-time calculation, respectively) are calculated (Figs. 6(b) and 6(c)). In Fig. 6(b), the $\rho_{EX}^{SCF}(\mathbf{r})$ is obtained from the occupation of $\pi^1\pi^*(\text{LUMO})^1$. Both density difference maps show the decrease of the electron density in π orbital and the increase of the electron density in π^* orbital. Thus, we can conclude that the absorption peak at 7.65 eV corresponds to the $\pi \rightarrow \pi^*$ excitation. Also, we assigned the peak at ~6.1 eV by using the same method as before (Fig. 6(c)). In this case, we applied the corresponding harmonic field along the x-direction and the $\rho_{EX}^{SCF}(\mathbf{r})$ is calculated from the occupation of $\pi^1 4a_g(\text{LUMO} + 1)^1$. Thus, we can conclude that the transition at ~6.1 eV corresponds to the $\pi \rightarrow 4a_g$ excitation. It is known that this type of excitation is highly related to delocalized Rydberg-type excitation.[44] The former study based on the wavefunction theories also predicted the two lowest bright states at approximately 6 eV and 7.8 eV, and provided the assignment as $\pi \rightarrow 3s$ and $\pi \rightarrow \pi^*$ excitations, respectively.[45,46] While the wavefunction theory provides the delocalized Rydberg state properly, the current study underestimates the delocalization of electron density even though the excitation energy is correct. This localized nature shown in the calculated density difference map results from the well-known TDDFT issue that it cannot suitably describe Rydberg excitations.[47] Thus, the exact behavior of density cannot be shown correctly in TDDFT regime. However, we expect that a strong electric field enough to tunnel out a portion of electron density mimics Rydberg excitations.

C. The effect of nucleus motion on absorption spectrum

Considering that the time evolution has been performed up to several femtoseconds, the nucleus dynamics should be considered. To calculate nuclear vibration coupled electronic spectra, we calculate the electronic spectra while the nuclei move classically on an electronic potential energy surface. In other words, the Ehrenfest dynamics[38] is implemented in the framework of the RT-TDDFT even though the Ehrenfest dynamics has a difficulty in handling the complex potential energy surface such as a conical intersection. The classical dynamics of nuclei was implemented by the Verlet algorithm. In the TDDFT framework, the time dependent external potential includes the time dependent potential from the motion of nuclei as well as the time dependent electric field. In the absence of any time dependent external electric field, the motion of electron density is affected by only the motion of nuclei. Thus, from the ground state, the electron density follows the ground state to the accuracy given by the exchange-correlation functional in the case that the trajectory does not touch any conical intersection. There are many efforts to improve the exchange correlation functional by including the memory effect and frequency-dependent terms.[2,48] Also, we should mention that the linear response time dependent density functional theory alone has a difficulty to deal with conical intersections at the current stage.[49] When a time dependent electric field exists, the electron density formed by a mixture of various states follows a mixed potential energy surface. Since the motion of nuclei consists of various normal modes which have specific frequencies, the motion of electron density is coupled to the motion of nuclei. Noting that the normal time step size for electron dynamics is several attoseconds, the calculation of forces on nuclei at every time step is inefficient since the position of nuclei does not change significantly within several attoseconds. In this sense, we introduce a time step size for nuclei (Δt_n) which is several multiples of the electronic time step Δt. Then, the force is calculated with the period of Δt_n. For the intermediate time, the position of nuclei is assumed by the uniform acceleration motion.

We investigated the effect of nucleus motion on absorption spectra for an ethylene molecule as an application of this coupled electron-nucleus dynamics. Applying a z-directional electric field, the coupled electron-nucleus dynamics was performed at 300 K up to 150 fs with random initial velocities. We calculated the electronic spectrum of an ethylene molecule with both $\Delta t_n = 1.44$ fs and $\Delta t_n = 0.29$ fs. Since the electron density rapidly oscillates with a period of several hundreds of attoseconds, forces from the time dependent density should be calculated with a small time step size. We compare the calculated spectra below the ionization potential (10.50 eV) with the experimental one measured at room temperature[50] in Fig. 7. The smaller time step size for nuclei gives a more similar result to the experimental spectrum. The experiment shows two sets of absorption peaks which consist of peaks apart by ~200 meV with each other (set A) and their side peaks blue-shifted by ~70 meV from set A (set B). With a time step size of 1.44 fs, we can see only "set A" peaks clearly while a time step size of 0.29 fs gives "set B" peaks as well as "set A" peaks. We also tried to investigate the effect of constrained vibrational motion to the vibrational-electronic absorption spectra. In this case, we perturbed the position of nuclei slightly from the equilibrium position so that the perturbation gives the motion of specific nuclear vibration. Here, we excited the four vibrational motions: CC stretching, CH stretching, CH wagging, and twisting modes by changing R_{CC}, R_{CH}, α, and β, respectively. Figure 8 shows the dependency of the π-π^* excitation peak on the normal mode vibrations. Both CC and CH stretching modes give several absorption peaks ~200 meV apart. Here, ~200 meV corresponds to the frequency of CC stretching motions. For the case of CH stretching, the CC

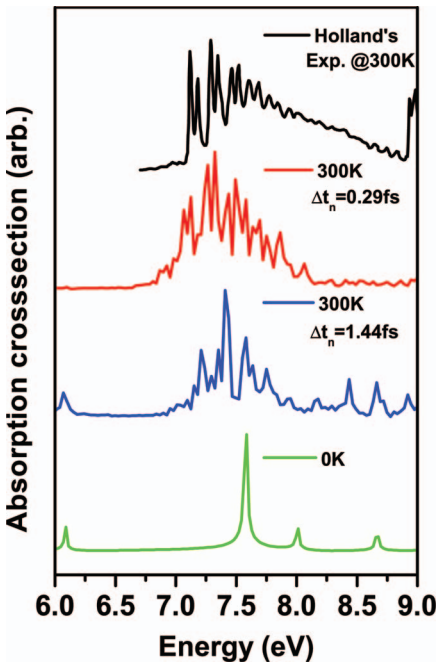

FIG. 7. The absorption spectra from Holland's experiment (black), the coupled electron-nucleus dynamics at 300 K with a nuclear time step size as 0.29 fs (red) and 1.44 fs (blue), and the electron dynamics (green).

stretching mode is slightly excited, i.e., CH stretching induces CC bonds to vibrate, so that small peaks appear compared to CC stretching. However, if CH wagging and twisting modes are excited, the side peaks emerge in addition to CC splitting peaks. Here, we can conclude that the out-of-plane motions of nuclei give rise to side peaks associated with the peaks from the CC stretching motion. Compared to the result from the multiple spawning methods which can treat nuclei as quantum particles,[31,45,46] the study based on the classical dynamics also shows a good agreement with experimental results since the absorption spectrum of an ethylene molecule is determined in the potential energy surfaces which is distant from conical intersections. In the case that the non-adiabaticity is important, the classical treatment of nuclear motions would be questionable.

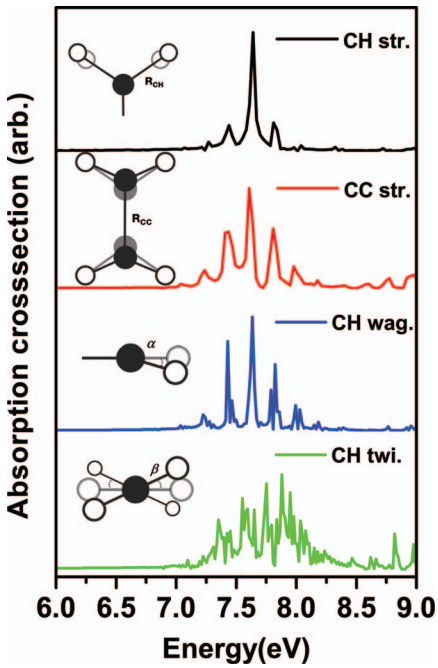

FIG. 8. The constrained-nuclear-vibration coupled electronic absorption spectra with CH stretching (black), CC stretching (red), CH wagging (blue), and CH twisting (green) excitations, respectively.

D. Excited state dynamics

As another application, we describe the excited state dynamics of a hydrogen molecule (H_2) as the simplest example in Fig. 9. From the first excited state obtained by optimizing the electron density with occupancy ($\sigma^1\sigma^{*1}$), we investigated the adiabatic dynamics of both electron density and nuclei with the adiabatic local spin density approximation (ALSDA) and the Troullier-Martins PPs. In this case, the total energy is conserved within a numerical error of 5.8×10^{-5} Ry. The excitation energy is transferred to the kinetic energy of nuclei, which was zero initially. The electron-electron repulsion triggers the dissociation of the H_2 molecule. We also calculated the self-consistent electronic energy with the excited state occupancy ($\sigma^1\sigma^{*1}$) for each structure in time. From the potential energy curve, we can conclude that the real-time electron density follows the excited state potential energy curve, and two separated hydrogen atoms are formed within a few femtoseconds.

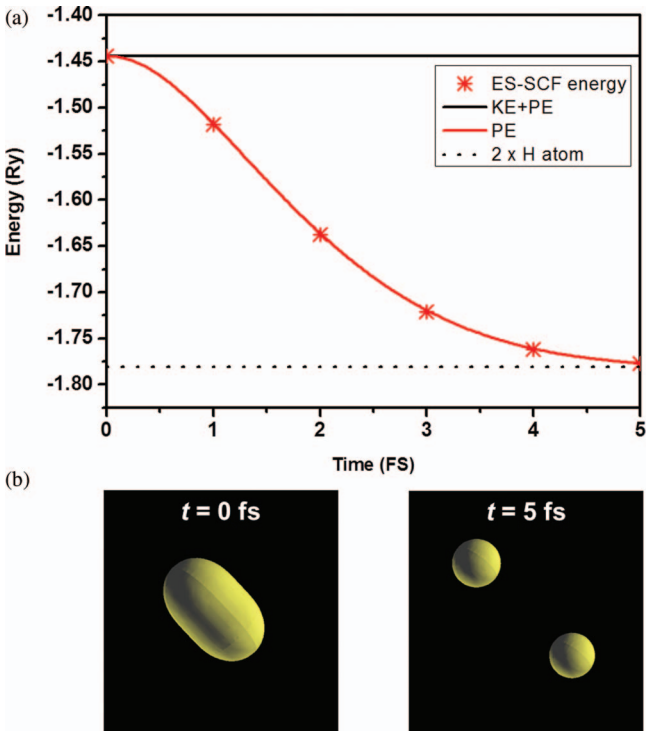

FIG. 9. (a) The energy curves for the adiabatic coupled electron-nucleus dynamics for the dissociation of the $\sigma \rightarrow \sigma^*$ excited hydrogen molecule. The coupled electron-nucleus dynamics follows the excited state potential energy. (b) The electron density after Frank-Condon excitation (left) and the electron density after the dissociation completes.

IV. CONCLUSION

In this paper, we implemented the twice faster algorithm for the RT-TDDFT with the complex ST_3 propagator into the PW-based DFT code. The ST_3 gives competitive results with the more time-consuming high order ST_4. As a test application, the RT-TDDFT-based absorption spectrum of an ethylene molecule was calculated. Compared to the well-developed LR-TDDFT result, the RT-TDDFT absorption spectrum is very similar to the linear response absorption spectrum. Furthermore, implementing the coupled electron-nucleus dynamics within the Ehrenfest dynamics regime, we obtained a molecular vibration-coupled absorption spectrum. At room temperature, the nucleus vibrational motion splits a single absorption peak into several vibration-coupled absorption peaks, showing the fine structure which is very similar to the experiment. As another application for the excited state dynamics, the adiabatic dynamics of the $\sigma \rightarrow \sigma^*$ excited hydrogen molecule shows dissociation of H_2 following the potential energy curve of the excited state. The efficient ST_3 propagator is found to be much favorable for a long time electron dynamics simulation.

ACKNOWLEDGMENTS

This work was supported by NRF (National Honor Scientist Program: 2010-0020414, WCU: R32-2008-000-10180-0), and KISTI (KSC-2011-G3-02).

[1] M. van Schilfgaarde, T. Kotani, and S. Faleev, Phys. Rev. Lett. **96**, 226402 (2006).
[2] G. Onida, L. Reining, and A. Rubio, Rev. Mod. Phys. **74**, 601 (2002).
[3] E. K. U. Gross and W. Kohn, Phys. Rev. Lett. **55**, 2850 (1985).
[4] M. E. Casida, in *Recent Advances in Density Functional Methods*, Edited by D. P. Chong (World Scientific, Singapore, 1995), Vol. 1.
[5] M. K. Nazeeruddin, F. de Argelis, S. Fantacci, A. Selloni, G. Viscardi, P. Liska, S. Ito, B. Takeru, and M. Grätzel, J. Am. Chem. Soc. **127**, 16835 (2005).
[6] M. Kolaski, H. M. Lee, C. Pak, and K. S. Kim, J. Am. Chem. Soc. **130**, 103 (2008).
[7] D. Majumdar, J. Kim, and K. S. Kim, J. Chem. Phys. **112**, 101 (2000).
[8] D. Majumdar, H. M. Lee, J. Kim, and K. S. Kim, J. Chem. Phys. **111**, 5866 (1999).
[9] N. T. Maitra, J. Chem. Phys. **122**, 234104 (2005).
[10] A. Dreuw and M. Head-Gordon, J. Am. Chem. Soc. **126**, 4007 (2004).
[11] O. Gritsenko and E. J. Baerends, J. Chem. Phys. **121**, 655 (2004).
[12] K. Yabana, T. Nakatsukasa, J.-I. Iwata, and G. F. Bertsch, Phys. Status Solidi B **243**, 1121 (2006).
[13] K. Yabana and G. F. Bertsch, Phys. Rev. B **54**, 4484 (1996).
[14] A. Castro, H. Appel, M. Oliveira, C. A. Rozzi, X. Andrade, F. Lorenzen, M. A. L. Marques, E. K. U. Gross, and A. Rubio, Phys. Status Solidi B **243**, 2465 (2006).
[15] M. A. L. Marques, X. Lopez, D. Varsano, A. Castro, and A. Rubio, Phys. Rev. Lett. **90**, 258101 (2003).
[16] O. Sugino and Y. Miyamoto, Phys. Rev. B **59**, 2579 (1999).
[17] O. Sugino and Y. Miyamoto, Phys. Rev. B **66**, 089901 (2002).
[18] H. Zhang and Y. Miyamoto, Appl. Phys. Lett. **95**, 053109 (2009).
[19] Y. Miyamoto, H. Zhang, and A. Rubio, Phys. Rev. Lett. **105**, 248301 (2010).
[20] T. Kunert, F. Grossmann, and R. Schmidt, Phys. Rev. A **72**, 023422 (2005).
[21] H. Chen, J. McMahon, M. A. Ratner, and G. C. Schatz, J. Phys. Chem. C **114**, 14384 (2010).
[22] K. Lopata and N. Govind, J. Chem. Theory Comput. **7**, 1344 (2011).
[23] T. Akama and H. Nakai, J. Chem. Phys. **132**, 054104 (2010).
[24] X. Li, S. M. Smith, A. N. Markevitch, D. A. Romanov, R. J. Levis, and H. B. Schlegel, Phys. Chem. Chem. Phys. **7**, 233 (2005).
[25] S. Meng and E. Kaxiras, J. Chem. Phys. **129**, 054110 (2008).
[26] W. Stier and O. V. Prezhdo, J. Phys. Chem. B **106**, 8047 (2002).
[27] E. Runge and E. K. U. Gross, Phys. Rev. Lett. **52**, 997 (1984).
[28] M. Drescher, M. Hentschel, R. Kienberger, M. Uiberacker, V. Yakovlev, A. Scrinzi, Th. Westerwalbesloh, U. Kleinberg, U. Heinzmann, and F. Krausz, Nature (London) **419**, 803 (2002).
[29] S. Baker, J. S. Robinson, C. A. Haworth, H. Teng, R. A. Smith, C. C. Chirilă, M. Lein, J. W. G. Tisch, and J. P. Marangos, Science **312**, 424 (2006).
[30] F. Krausz and M. Ivanov, Rev. Mod. Phys. **81**, 163 (2009).
[31] M. Ben-Nun, J. Quenneville, and T. J. Martinez, J. Phys. Chem. A **104**, 5161 (2000).
[32] M. Ben-Nun and T. J. Martinez, J. Chem. Phys. **108**, 7244 (1998).
[33] J. C. Tully, J. Chem. Phys. **93**, 1061 (1990).
[34] Y. Miyamoto and H. Zhang, Phys. Rev. B **77**, 165123 (2008).
[35] P. Giannozzi, S. Baroni, N. Bonini, M. Calandra, R. Car, C. Cavazzoni, D. Ceresoli, G. L. Chiarotti, M. Cococcioni, I. Dabo, A. Dal Corso, S. Fabris, G. Fratesi, S. de Gironcoli, R. Gebauer, U. Gerstmann, C. Gougoussis, A. Kokalj, M. Lazzeri, L. Martin-Samos, N. Marzari, F. Mauri, R. Mazzarello, S. Paolini, A. Pasquarello, L. Paulatto, C. Sbraccia, S. Scandolo, G. Sclauzero, A. P. Seitsonen, A. Smogunov, P. Umari, and R. M. Wentzcovitch, J. Phys.: Condens. Matter **21**, 395502 (2009).
[36] T. Prosen and I. Pižorn, J. Phys. A **39**, 5957 (2006).
[37] M. Suzuki and T. Yamauchi, J. Math. Phys. **34**, 4892 (1993).
[38] A. P. Horsfield, D. R. Bowler, and A. J. Fisher, J. Phys.: Condens. Matter **16**, L65 (2004).
[39] J. P. Perdew and A. Zunger, Phys. Rev. B **23**, 5048 (1981).
[40] A. Castro, M. A. L. Marques, and A. Rubio, J. Chem. Phys. **121**, 3425 (2004).
[41] D. Vanderbilt, Phys. Rev. B **41**, 7892 (1990).
[42] N. Troullier and J. L. Martins, Solid State Commun. **74**, 613 (1990).
[43] A. Marini, C. Hogan, M. Gruning, and D. Varsano, Comput. Phys. Commun. **180**, 1392 (2009).
[44] A. J. Merer and R. S. Mulliken, Chem. Rev. **69**, 639 (1969).
[45] K. K. Baeck and T. J. Martinez, Chem. Phys. Lett. **375**, 299 (2003).
[46] M. Ben-Nun and T. J. Martinez, J. Phys. Chem. A **103**, 10517 (1999).
[47] M. Ben-Nun and T. J. Martinez, Chem. Phys. **259**, 237 (2000).
[48] N. T. Maitra, K. Burke, and C. Woodward, Phys. Rev. Lett. **89**, 023002 (2002).
[49] B. G. Levine, C. Ko, J. Quenneville, and T. J. Martinez, Mol. Phys. **104**, 1039 (2006).
[50] D. M. P. Holland, D. A. Shaw, M. A. Hayes, L. G. Shpinkova, E. E. Rennie, L. Karlsson, P. Baltzer, and B. Wannberg, Chem. Phys. **219**, 91 (1997).